Building and Environment 204 (2021) 108138

Contents lists available at ScienceDirect

Building and Environment

journal homepage: www.elsevier.com/locate/buildenv

Impacts of land use/ land cover types on interactions between urban heat island effects and heat waves

Zhendong Zou [1], Chunhua Yan [1], Leiyu Yu, Xianchenghao Jiang, Jinshan Ding, Longjun Qin, Bei Wang, Guoyu Qiu [*]

School of Environment and Energy, Peking University Shenzhen Graduate School, Shenzhen, 518055, China

ARTICLE INFO

Keywords:
Urban heat island
Heat wave
Interactions
LULC types
Natural underlying surface
Latent heat

ABSTRACT

The urban heat island (UHI) effect is a widespread phenomenon because of increased urbanization, making the urban thermal environment less comfortable. The UHI effect may worsen during heat waves (HWs), with projected increases in extreme climatic events in the future due to global warming. Researchers have revealed interactions between the UHI effect and HWs using weather station data and proposed mitigation schemes at a city scale. However, the UHI effect in urban areas with different land use/land cover (LULC) types should respond differently to HWs, which has drawn little attention. Hence, this study conducted a mobile transect experiment in the subtropical megacity of Shenzhen and obtained high spatial resolution data. The results showed that the UHI effect was significantly amplified during HWs. The UHI intensity (UHII) of the transect increased from 0.56 ± 0.50 °C under non-heat wave (NHW) conditions to 0.68 ± 0.65 °C during HWs. LULC types had a significant influence on this interaction. The UHII in more urbanized areas increased during HWs, whereas less urbanized areas had improved cooling effects. These interactions were more evident at nighttime. Increasing the natural underlying surface coverage mitigated the intensity and warming potential of the UHI effect. With a 10% increase in the natural underlying surface coverage, the nighttime UHII decreased by 0.38 °C and 0.39 °C during NHWs and HWs, respectively. These cooling effects were attributed to the increased latent heat consumption during HWs by vegetation. Therefore, different measures should be taken in other areas to mitigate UHII amplification during HWs.

1. Introduction

During the 19th century, only 10% of the world's population lived in urban areas; however, the urban population has now reached 55.3% and may increase to 68.4% by 2050 [1,2]. During rapid urbanization, large areas of high-permeable natural underlying surfaces are replaced by low-permeable artificial surfaces. Thus, the surface energy balance is altered, eventually causing the urban heat island (UHI) effect [3,4]. The UHI effect has been a great threat to urban residents because it makes them endure higher temperatures than people living in the surrounding rural areas [5,6]. Air conditioners consume large amounts of energy and increase the financial burden in many areas [7,8]. In addition, air conditioners releasing large amounts of heat into the environment further increases the outdoor air temperature [9,10]. Therefore, it is essential to investigate these critical problems with efficient measures to mitigate the UHI effect.

Heat waves (HWs), mesoscale events that bring warm air from the upper atmosphere [11,12], are a great threat to people in urban and rural areas. HWs can increase mortality during hot summers [13,14]. According to some predictions, HWs will be more frequent in the future due to continuous global warming and urbanization [15–18]. Therefore, it is essential to better understand the combined effects of the UHI and HWs, and their driving forces for mitigation strategies in response to climate change.

In most studies, the UHI effect was significantly exacerbated during HWs. For instance, Ramamurthy and Bou-Zeid [19] found enhanced UHI effects during HWs in New York City, Washington, DC, and Baltimore. The daily average UHI effect in New York City increased 1.5 °C during HWs [20]. Exacerbated UHI effects were also found in Beijing, Shanghai, and Guangzhou during HWs; however, the UHI effect in Shanghai had greater intensity during the daytime, whereas in Beijing and Guangzhou, it was greater during the nighttime [21]. The UHI intensity (UHII)

* Corresponding author.
E-mail address: qiugy@pkusz.edu.cn (G. Qiu).
[1] These authors contributed equally to this work.

https://doi.org/10.1016/j.buildenv.2021.108138
Received 7 May 2021; Received in revised form 7 July 2021; Accepted 9 July 2021
Available online 11 July 2021

increased by 0.78 °C during HW episodes in Beijing, which showed a greater increase at nighttime than daytime [22]. Prior research based on long-term data showed that in Karachi, the maximum difference in the UHII during HW and non-heat wave (NHW) periods was 2.5 °C–3 °C with the inclusion of different rural areas [23]. Within the urban area of Szeged, Hungary, the UHII was amplified by approximately 1–3 °C during a HW [24]. However, other studies have found no amplification of UHII during HWs [25]. One study focused on 54 cities in the United States based on data from 2000 to 2015, and documented that the differences in daily minimum or maximum temperatures between urban and rural stations decreased with increasing temperature in most cities (38/54) [26]. Cities in temperate climate regions showed significant synergistic effects between UHI effects and HWs, whereas this synergistic effect was insignificant for cities in dry regions [27]. A similar phenomenon was found in China, where the contribution of urbanization to HWs was stronger in wet climates, whereas it was smaller and even negative in arid regions [28]. These contradictory conclusions require further investigation.

Previous studies showed that UHII varies across different LULC types when HWs and NHWs were not distinguished [29–31]. More urbanized areas, such as commercial center and industrial areas, got higher UHII [32,33]. Less urbanized areas, such as parks, got lower UHII on the contrary [34,35]. UHI effects differ in different urban areas due to different energy exchange processes [36–39], which should also response differently to HWs. Recently. A study found that compared with regular episodes, urbanization-induced changes in latent heat and sensible heat fluxes are more significant throughout most of the day during the heatwave episode [22]. It indicates that the LULC types would affect the energy balance changes and thus affect the UHII changes from NHWs to HWs. Actually, several studies also found different interactions between UHII and HWs in different LULC types [21,25]. However, these differences were just described qualitatively instead of systematic analysis. Most of related studies focused on the impacts of meteorological factors such as wind velocity and relative humidity, instead [40,41]. The meteorological factors among different sites in these studies were quite different, thus showing greater impacts on the interactions of UHII and HWs. As a result, the impacts of LULC types have been usually neglected and not quantitatively revealed.

Besides, almost all recent studies have investigated the interactions using direct application or simulation (e.g., WRF) based on weather station data. However, the land surface schemes in the default WRF use surface layer similarity theory, which fails in dense urban environments [19,20]. Moreover, weather stations are mostly located in open landscapes (World Meteorological Organization standard), which are similar to rural environments [27]. The number of weather stations is also limited and could not accurately reveal the heterogeneity of urban areas, which is the most prominent characteristics of urban areas. Consequently, it remains challenging to describe the UHI effect of a city precisely based only on weather station data. The proposed mitigation measures on the city scale are also hard to apply to all blocks with different LULC types directly.

Therefore, the present study first determined how UHII interacts with HWs in the subtropical coastal megacity of Shenzhen. We then focused on this interaction in different areas within the urban area, with high temporal and spatial resolution data of temperature based on mobile transect experiments. We aimed to reveal the impacts of land use/land cover (LULC) types on these interactions, and obtain clues for mitigating the UHI effect during HWs at a higher spatial resolution. The UHI effect results from replacing the natural underlying surface with an artificial underlying surface; thus, the natural underlying surface coverage is hypothesized to influence the interactions discussed above. To verify this, the relationship between UHII and the coverage of the natural underlying surface in all 26 sections was also investigated. High atmospheric relative humidity (RH) puts more heat stress on the human body under HWs [42]. The apparent temperature (AT), representing the combined effects of temperature and humidity [43], was thus also analyzed in the present study to better reveal the heat stress on human body changes during HWs.

2. Materials and methods

2.1. Study area

The transect was set in Xili, Nanshan District, Shenzhen, China. Shenzhen (113°45′44″ E–114°37′21″ E, 22°26′59″ N–22°51′49″ N) is a coastal megacity that is characterized by a subtropical humid climate. The mean annual air temperature is 23 °C, and the average temperature of the hottest month (July) reaches 28.9 °C. The perennial mean precipitation is 1935.8 mm, of which 86% occurs between April and September. The perennial mean wind speed is 2.7 m s^{-1}, and is lower in summer than during other seasons. Shenzhen is affected by tropical cyclones four to five times each year.

It has taken approximately 40 years for Shenzhen to grow from a small village to become one of the largest cities in southern China. The permanent population in Shenzhen was 13.03 million at the end of 2018, with a population density of 6484 persons per square kilometer. The transect in the present study was set in Nanshan District, which contributes the highest gross domestic product to Shenzhen. According to our previous study, the UHII of this district was almost the same as that of the entire Shenzhen [44]. The transect used was 8 km long, with an altitude of approximately 20 m. The air temperature along the transect is believed to be affected by a 150-m wide area on each side of the transect, and was determined to be 100 times the height of the air temperature measurement based on the fetch requirement for meteorological measurements [45,46]. Therefore, the experimental area was 300 m wide and 8 km long. This area included a variety of land cover types (Fig. 1), with woodland, grassland, water bodies (lakes and rivers), and bare land classified into natural underlying surfaces, whereas paved roads, buildings (residential and commercial buildings), and paved surfaces (concrete pavement and brick pavement) were classified as artificial underlying surfaces. Based on the similarity of vegetation coverage and land cover types, the transect was divided into 47 sites. They were further divided into 26 sections when land use type, vegetation types, growth status, road width, building usage, and building height were considered (Table 1). For example, though P1 to P5 were all classified as land for education, the coverages of each land cover type were quite different. At P1, the coverage of buildings, paved surfaces, grasslands and woodlands were about 25.68%, 4.65%, 24.43% and 30.72%, while at P2 they were 17.66%, 9.90%, 10.86% and 45.61%, and at P5 they were 6.40%, 20.76%, 31.11% and 22.94%. Besides, the woodland at P1 was mainly covered by *Grevillea robusta*, *Karaya gum*, *Albizia falcataria*, *Swietenia mahogany* and *Eucalyptus robusta*, while at P2 were *Bambusa textilis*, *Delonix regia* and *Swietenia mahogany*. The area of each land cover type was obtained by ground investigation and Google Earth images (pixel resolution of 4 m). Then its coverages in each section was defined as the ratio of its area to that of the section. Therefore, the natural underlying surface coverage is the total coverage of woodland, lawn, water bodies and bare land. The transect has been described in more detail in our previous study [47,48].

2.2. Data sets

The experiment was conducted using an e-bike once every 2 h, except for during rain events, from July 2011 to June 2013. Each observation lasted approximately 30 min, and 7011 measurements were taken during the two years. A Cu–Co thermal couple (resolution 0.01 °C) and an HPM60 sensor (Vaisala, Finland, resolution 0.01%) were installed in a sleeve, which was made of two different sizes of white PVC tubes (with length/diameter/thickness of 250/80/3 mm and 230/55/2 mm, respectively), to record the air temperature and RH. A GPS device (GPS16X–HVS, Campbell Scientific Inc., USA, resolution 0.6″) was installed to record the location. All data were sampled every 5 s and

Fig. 1. Study area, observation transect, and observation sites. The length and width of the transect were 8 km and 300 m, respectively. A total of 47 sites were included based on the similarity of vegetation coverage and land use type. The observation sites were assembled into 26 sections based on their similarities. Mobile traverse observations were conducted by the pictured auto bike and mounted equipment [48]. The street views of four typical sections are also shown (P1: site 1 to 2; P14: site 25 to 26; P19: site 35 to 36; P22: site 40 to 41).

recorded using a CR1000 data logger (Campbell Scientific Inc., USA). The small time lag effect among the different sites along the transect on temperature and RH measurements could be neglected [48]. For all 7011 measurements, similar temperature and RH values were found at P1, which was the start and end site for each observation (air temperature, $p = 0.995$ and RH, $p = 0.174$, by independent sample *t*-test). The air temperature between July 2011 and June 2013 from the Xili meteorological station (where the transect was located) was collected to define HWs and NHWs for the study area.

In addition, we conducted evapotranspiration measurements of a lawn (*Zoysia matrella*) and a tree (*Ficus concinna*) at the beginning of the transect (P2), to explain the different cool island effects of evapotranspiration in NHWs to HWs. The evapotranspiration rate of the lawn was measured by a Bowen ratio system and the transpiration rate of the tree was measured by a sap flow system (SF-G type probes, Ecomatic, Munich, Germany). Details of these measurements were introduced in our previous researches [49,50].

2.3. HW definition

According to the Chinese Meteorology Administration, a HW is defined as a period of at least three consecutive days with a daily maximum temperature reaching 35 °C. In our study period, six HWs occurred on 2011/8/2 to 2011/8/4, 2011/8/29 to 2011/8/31, 2012/7/19 to 2012/7/21, 2012/7/30 to 2012/8/2, 2012/8/7 to 2012/8/9, and 2013/6/19 to 2013/6/21. The last HW was not included in the present study because a large part of the simultaneous transect observation data was missing due to device malfunction. Therefore, only the first five HWs are discussed below.

An NHW is defined as the total 30 day period before and after each HW period. For example, 2011/7/19 to 2011/8/1 and 2011/8/5 to 2011/8/18 are defined as the NHW period for the HW period from 2011/8/2 to 2011/8/4. To diminish the effect of weather conditions on the comparison of UHI effects between HWs and NHWs, precipitation days (daily precipitation over 0.1 mm) were excluded [21].

Day and night were divided based on sunrise and sunset times in Shenzhen, with daytime defined as the time between 6:00 and 18:00, and nighttime as 20:00 to 4:00 local standard time [47].

2.4. Parameter calculation and statistical analysis

UHII is defined as the temperature difference between urban areas

and adjacent suburban settings, as follows:

$$UHII = T_u - T_s \quad (1)$$

where, T_u and T_s denote the urban and suburban temperatures, respectively. In our study, P9 was selected as the suburban area because it had the highest forest cover, with a natural underlying surface coverage up to 83.13%.

The AT was calculated based on the Rothfusz regression [23,51]:

$$AT_F = -42.379 + 2.049T + 10.143(RH) - 0.2247(T)(RH) - 6.83 \times 10^{-3}T^2 - 5.48 \times 10^{-2}(RH)^2 + 1.22 \times 10^{-3}(T)^2(RH) + 8.5 \times 10^{-4}(T)(RH)^2 - 1.99 \times 10^{-6}T^2(RH)^2 \quad (2)$$

Table 1
Characteristics of observation sections and sites over the 8 km transect. Land cover types were not shown as almost all sites contained those 7 land cover types, including woodland, grassland, water bodies, bare land, paved roads, buildings and paved surfaces. The site numbers are explained in Fig. 1 [48].

Section	Site	Land use type	Description	Natural underlying surface coverage	Section	Site	Land use type	Description	Natural underlying surface coverage
P1	1–2	Land for education	Campus and a golf course	58.83%	P14	25–26	Residential land	Narrow road in urban village	14.16%
P2	3–4	Land for education	Campus and a golf course	61.59%	P15	27–28	Residential land	Urban village	18.82%
P3	5–6	Land for education	On campus, planted forest	59.88%	P16	29–30	Industrial land	Planted forest, next to bare ground	32.67%
P4	7–8	Land for education	On campus, planted forest	57.20%	P17	31–32	Industrial land (to be developed)	Bridge over a lake	22.23%
P5	9–10	Land for education	On campus, a river	64.36%	P18	33–34	Retail commercial land	Busy roads in commercial center	12.04%
P6	10–11	Woodland	On campus, planted forest	74.67%	P19	35–36	Retail commercial land	Busy roads in commercial center	12.43%
P7	11–12	Woodland	On campus, planted lake	80.12%	P20	37–38	Retail commercial land	Busy roads in commercial center	22.73%
P8	13–14	Woodland	On campus, planted forest	79.25%	P21	38–39	Residential land/Land for education	Busy roads, with lush planted forest	52.77%
P9[a]	15–16	Woodland	On campus, planted forest	83.13%	P22	40–41	Land for public facilities	Busy roads, with lush planted forest	62.57%
P10	17–18	Woodland	Planted forest	64.47%	P23	41–42	Residential land	Busy roads, with lush planted forest	60.34%
P11	19–20	Woodland	Planted forest	55.40%	P24	42–43	Residential land	Residential area, planted forest	46.26%
P12	21–22	Residential land	Busy roads with planted trees	28.83%	P25	44–45	Land for education/ Parks and green fields	Campus and wildlife park	38.65%
P13	23–24	Residential land	Urban village	22.79%	P26	46–47	Land for education	Campus and a golf course	57.23%

[a] P9 was selected to be the background section as it had the highest natural underlying surface coverage.

where, T is the air temperature in degrees Fahrenheit (℉) and RH is the relative humidity (%). AT_F is the heat index as the apparent temperature in degrees Fahrenheit (℉). To unify the units of heat index to air temperature and $UHII$, we converted the unit of heat index into degrees centigrade (°C) as follows:

$$AT = (AT_F - 32)/1.8 \quad (3)$$

where, AT is the heat index in degrees centigrade (°C).

Two-hourly UHII and AT values were calculated for each section and averaged as daily values, then averaged as values for one HW and NHW. The average values of the five HWs and NHWs were used for the subsequent analysis. Warming potential is defined as the variation of UHII and AT from NHWs to HWs in the present study.

The significance of differences in UHII and AT between HWs and NHWs was tested using paired-sample t-tests with SPSS 18.0.0 (IBM Corporation, New York, USA). Curve fitting was performed in Excel 2019 (Microsoft Corporation, Redmond, WA, USA). Statistical analyses of the fitting parameters were performed using the Eviews 8 software package for Windows (Eviews, HIS Global Inc., London, UK).

3. Results

3.1. Variation in temperature and UHI effects from the NHW to HW periods

As shown in Fig. 2a, the air temperature during HWs was higher than that during NHWs ($p < 0.001$, 95% confidence). The average air temperature of the transect was approximately 29.07 °C in NHWs, whereas it reached 30.33 °C during HWs. The 26 sections became warmer during HWs, with increases ranging from 1.03 °C (P1, land for education) to 1.52 °C (P19, retail commercial land). The air temperature in more urbanized areas (i.e., P12–P19, including residential land, industrial land and retail commercial land)) was always higher than that in the less urbanized areas, and increased more from NHWs to HWs (1.44 °C for more urbanized areas compared to 1.19 °C for the remainder). In contrast, the RH during HWs was lower than that during NHWs ($p < 0.001$, 95% confidence, Fig. 2b). The average RH of the transect during HWs and NHWs was 70.88% and 75.44%, respectively. The 26 sections became 3.31% (P5, land for education) to 5.60% (P25, land for education/parks and green fields) drier during the HW periods. The RH in more urbanized areas (P12–P19) decreased more from NHWs to HWs (5.12% compared to 4.32% for the remainder). The AT during HWs was 28.65 °C, whereas it was 27.58 °C during NHWs ($p < 0.001$, 95%

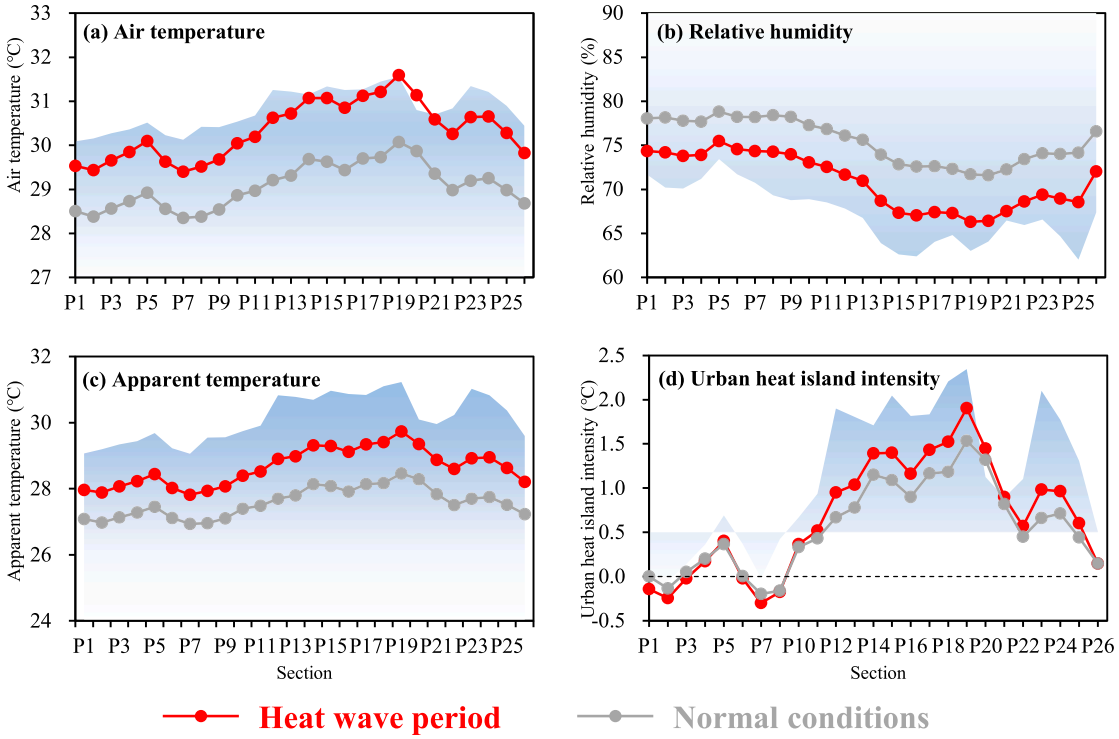

Fig. 2. Average air temperature (Ta; a), relative humidity (RH; b), apparent temperature (AT; c), and urban heat island intensity (UHII; d) of five heat waves (HWs) and non-heat waves (NHWs) for each section across the transect. The height of the blue shaded area indicates the amplitude of each parameter at each section from NHWs to HWs. The horizontal dashed line in (d) indicates a UHII of zero. (For interpretation of the references to colour in this figure legend, the reader is referred to the Web version of this article.)

confidence, Fig. 2c). Each section had a higher AT during HWs, varying from 0.88 °C to 1.27 °C. Sustained higher AT increases were observed in more urbanized areas from HWs to NHWs (1.21 °C), with lower values occurring in less urbanized areas (1.01 °C).

The average UHII of the transect increased from 0.56 °C during NHWs to 0.68 °C during HWs ($p = 0.001$, 95% confidence, Fig. 2d). Specifically, more urbanized areas had a larger UHII during HWs. For example, the UHII in the commercial center (P19, retail commercial land) and urban village (P14, residential land) was 0.37 °C and 0.24 °C larger in HWs than in NHWs, respectively. Well-vegetated areas, including P1–P3 and P6–P8 (land for education and woodlands, with average natural underlying surface of 60.10% and 78.01%, respectively), experienced greater cooling effects during HWs of −0.14 °C and −0.17 °C than NHWs with values of −0.03 °C and −0.12 °C, respectively. P1–P3 got lower temperature than P9 because the natural underlying surface there was high (58.83%–61.59%) and the roads there (one lane) were better shaded by buildings in the university campus. Since we rode the e-bike on the road to record the air temperature, this phenomenon was more evident in daytime (Fig. 3). During HWs, the shading effects could reduce more incoming energy, assuming the same shading coefficient for solar radiation, thus making the cold island effect in P1–P3 more evident. For P6–P8, their natural underlying surface coverage (74.67%–80.12%) were just slightly lower than that of P9. However, they'd gotten more coverage of water (1.31%–9.77%, while no water coverage at P9), which could cool down the air temperature more compared to vegetation transpiration [52]. Therefore, P6–P8 were cooler than P9. It was more evident at night when water evaporated but vegetation transpiration nearly stopped. (Fig. 3). This phenomenon might be enhanced during HWs as the temperature increases and water evaporates faster.

In general, the sections that already showed an intense UHI effect during NHWs were further increased during HWs. Similarly, sections that showed cooling effects or weak UHI effects during NHWs had stronger cooling effects during HWs. Therefore, the interactions between the UHI effect and HWs were different from the interactions between HWs and air temperature, RH, or AT. LULC types showed an evident influence on whether the UHII increased or decreased during HWs.

Table 2 shows the AT and UHII of different land use types in NHWs and HWs. The retail commercial land got the highest AT and strongest UHII both in NHWs and HWs. Woodland got the lowest AT and weakest UHII. Besides, the increase of AT and UHII from NHWs to HWs was also higher in residential land (1.20 °C and 0.28 °C), industrial land (1.20 °C and 0.27 °C) and retail commercial land (1.19 °C and 0.27 °C). The UHII of woodland did not increase in HWs. Land for education even got weaker UHII (0.05 °C). Different sections got different AT and UHII even they were classified into the same land use types. For example, AT and UHII of P14 and P15 were obviously higher than those of P23 and P24, though their land use types were all classified as residential land.

3.2. Interactions between HW and UHI effects in daytime and nighttime

As our previous study showed different characteristics of UHII during the daytime and nighttime [47], it was hypothesized that different interactions between UHI effects and HWs would occur at different times. Fig. 3a and b shows that daytime and nighttime UHII was mostly higher during HWs than NHWs. During HWs, daytime UHII across the transect ranged from −0.42 °C to 1.45 °C with a mean value of 0.47 °C, whereas the nighttime UHII ranged between −0.53 °C and 2.59 °C with a mean of 0.99 °C. Similarly, during NHWs, the daytime UHII across the transect varied from −0.29 °C to 1.17 °C, with a mean of 0.36 °C, and nighttime UHII at each section ranged between −0.22 °C and 2.04 °C, with a mean of 0.83 °C. The nighttime UHII was 0.52 °C higher than the daytime UHII during HWs, and the difference was 0.47 °C during NHWs. In addition, daytime and nighttime UHII increased by 0.11 °C and 0.16 °C, respectively, during HWs. Therefore, there was a larger amplification effect of

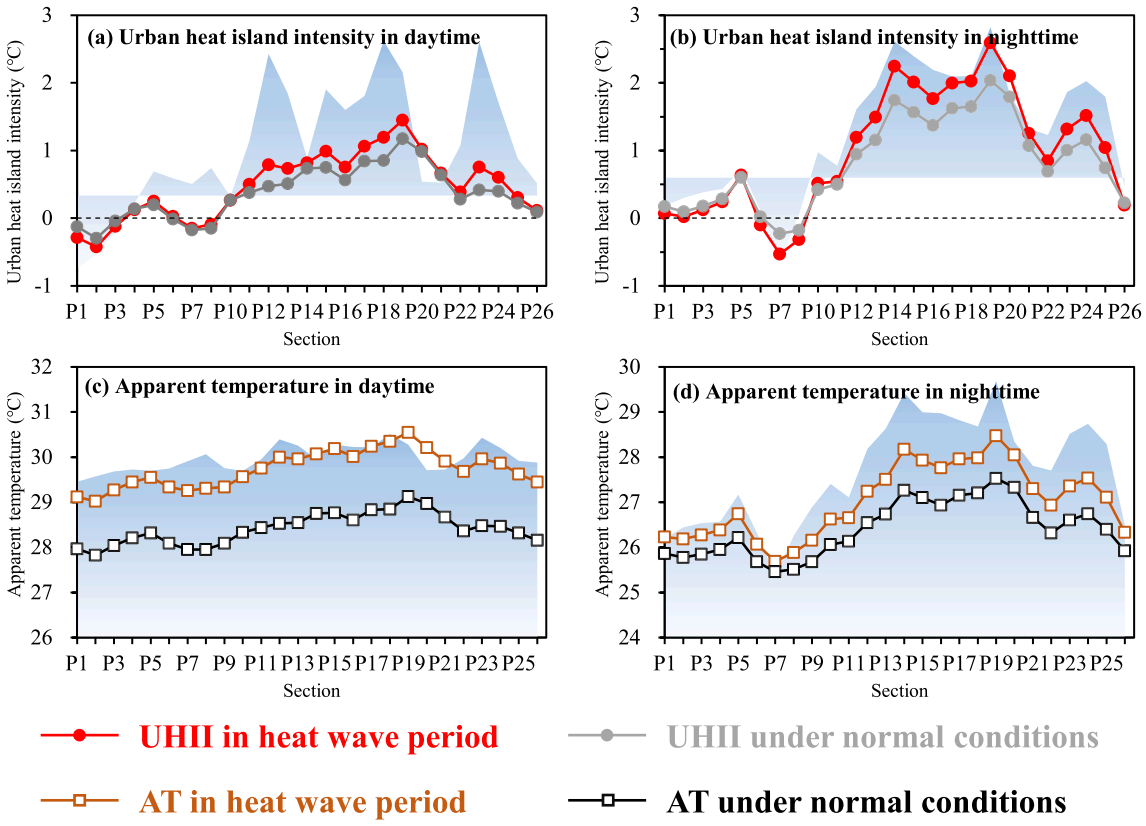

Fig. 3. Average urban heat island intensity (UHII; a, b) and apparent temperature (AT; c, d) of five heat waves (HWs) and non-heat waves (NHWs) during the daytime and nighttime for each section across the transect. The height of the blue shaded area indicates the amplitude of each parameter at each section from NHWs to HWs. The horizontal black dashed lines in (a) and (b) indicate a UHII of zero. (For interpretation of the references to colour in this figure legend, the reader is referred to the Web version of this article.)

HWs on UHII during the nighttime under intense UHI effects. The amplification effect of HWs varied among the different transect sections with various LULC types. A larger amplification occurred in more urbanized areas. For example, in the commercial center (P19, retail commercial land), the UHII increased from 1.17 °C to 1.45 °C during the daytime and 2.04 °C–2.59 °C during the nighttime. Similarly, for areas that experienced the cold island effect during NHWs, their cooling potentials were increased during HWs, especially at night. For instance, over well-vegetated areas (P6–P8, woodlands), UHII varied from −0.11 °C to −0.07 °C during the daytime (the cooling effect slightly decreased but still existed), and varied from −0.13 °C to −0.32 °C during the nighttime (the cooling effect was significantly intensified). Therefore, the UHI effect and cold island effect were exacerbated by HWs, and the amplification effect of HWs was governed by time and LULC type.

In contrast to the UHI effect, the AT increased during HWs regardless of whether it was a more or less urbanized area (Fig. 2c and d); therefore, there was greater heat stress for residents, especially during the daytime. The AT along the transect increased by 1.32 °C during the daytime (from 28.41 °C to 29.73 °C, Fig. 2c) and by 0.61 °C during the nighttime (from 26.41 °C to 27.02 °C, Fig. 2d). The amplification effect of HWs on AT was also governed by time and LULC type. For more urbanized areas, AT

Table 2
Air temperature, relative humidity, apparent temperature (AT) and urban heat island intensity (UHII) in different land use types.

LULC type	Section	AT (°C)		UHII (°C)		LULC type	Section	AT (°C)		UHII (°C)	
		NHWs	HWs	NHWs	HWs			NHWs	HWs	NHWs	HWs
Land for education	P3	27.13	28.07	0.05	−0.02	Woodland	P6	27.11	28.03	0.00	−0.02
	P4	27.28	28.23	0.20	0.17		P7	26.93	27.82	−0.20	−0.30
	P5	27.45	28.44	0.37	0.40		P8	26.96	27.93	−0.16	−0.18
	P1	27.08	27.97	0.00	−0.14		P9	27.10	28.07		
	P2	26.97	27.88	−0.13	−0.25		P10	27.39	28.40	0.33	0.37
	P26	27.23	28.21	0.15	0.15		P11	27.48	28.52	0.43	0.52
	average	**27.19**	**28.13**	**0.10**	**0.05**		**average**	**27.16**	**28.13**	**0.08**	**0.08**
Land for education/Parks and green fields	**P25**	**27.51**	**28.63**	**0.44**	**0.60**	Industrial land	P16	27.91	29.12	0.90	1.16
Residential land	P12	27.70	28.90	0.67	0.95		P17	28.14	29.34	1.17	1.43
	P13	27.80	28.98	0.78	1.04		**average**	**28.03**	**29.23**	**1.03**	**1.30**
	P14	28.14	29.31	1.15	1.39	Retail commercial land	P18	28.17	29.41	1.18	1.52
	P15	28.08	29.30	1.09	1.40		P19	28.47	29.73	1.53	1.90
	P23	27.70	28.92	0.66	0.98		P20	28.29	29.35	1.32	1.45
	P24	27.75	28.95	0.71	0.97		**Average**	**28.31**	**29.50**	**1.35**	**1.62**
	average	**27.86**	**29.06**	**0.84**	**1.12**	Land for public facilities	**P22**	**27.51**	**28.60**	**0.45**	**0.57**
Residential land/Land for education	**P21**	**27.83**	**28.87**	**0.82**	**0.90**						

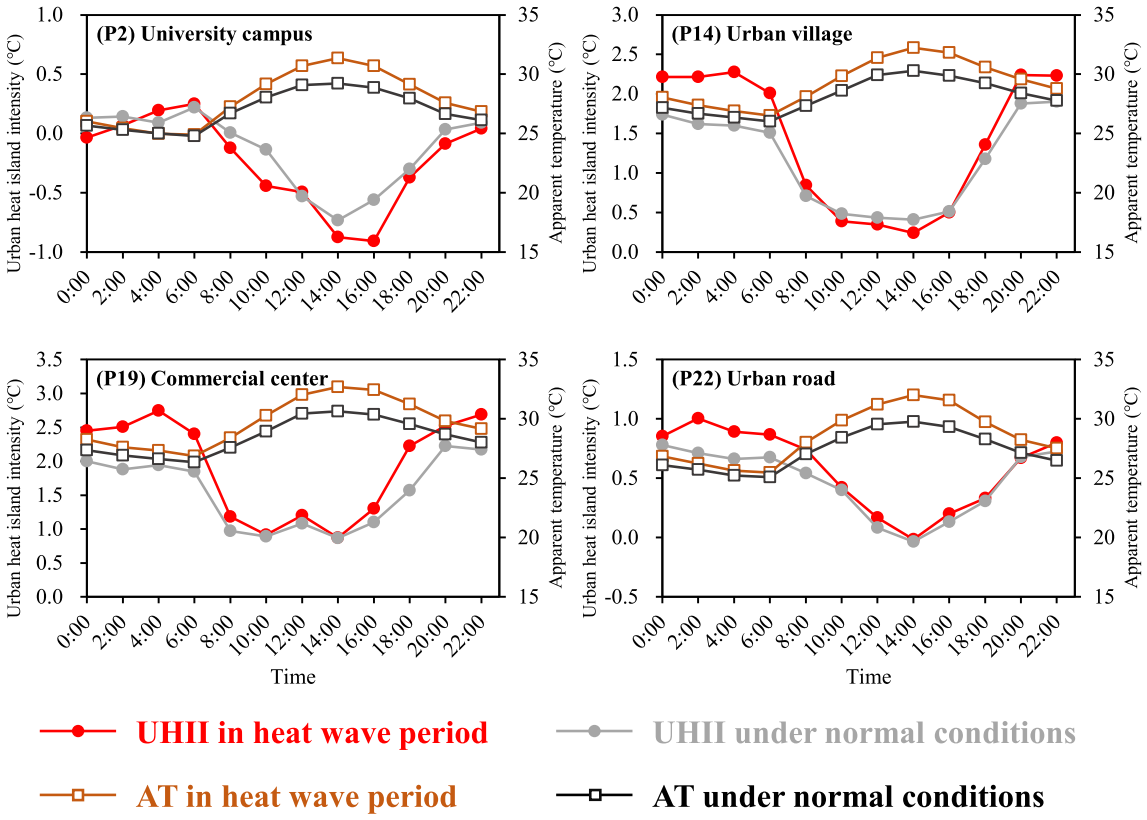

Fig. 4. Diurnal urban heat island intensity (UHII) and apparent temperature (AT) of four typical urban LULC types during heat wave (HWs) and non-heat waves (NHWs): (a) university campus; (b) urban village; (c) commercial center; and (d) urban road.

was increased by 1.42 °C during the daytime and 0.82 °C at nighttime during HWs. For less urbanized areas, AT was increased by 1.28 °C and 0.52 °C during the daytime and nighttime, respectively. Therefore, HWs caused greater heat stress in more urbanized areas, especially during the nighttime. HWs enhanced the UHII under higher UHII, and increased AT more when AT was higher, thereby making the thermal environment worse.

3.3. Interactions between HWs and UHI effects in areas with different LULC types

To clarify the influence of LULC types on the interactions between HWs and UHI effects, four sections with four typical LULC types (land for education, residential land, retail commercial land and land for public facilities) were selected for subsequent analysis. Sections with industrial land were not included because industry there were still to be developed. Overall, the diurnal UHII in the selected four sections showed similar patterns: higher in the nighttime and lower in the daytime (Fig. 4). The well-vegetated university campus (P2, land for education) showed an obvious cooling island effect between 8:00 and 18:00 during HWs and NHWs (Fig. 4a), and the cooling effect was greater in HWs (−0.23 °C) than in NHWs (−0.13 °C). From 20:00 to 6:00, when there was an UHI effect, the intensity was lower during HWs. This was different from the other three more urbanized areas. HWs enhanced the UHI effects greatly in the urban village (P14, residential land, Fig. 4b), commercial center (P19, retail commercial land, Fig. 4c), and urban road (P22, land for public facilities, Fig. 4d), increasing from 1.16 °C, 1.55 °C, and 0.47 °C during NHWs to 1.41 °C, 1.92 °C, and 0.58 °C during HWs, respectively. The intensity and increase of the UHII for the urban road were lower than those in the urban village and commercial center because the road was well vegetated. The increase in UHII during HWs in the urban village and commercial center was more dramatic at night (i.e., 20:00 to 6:00), when the UHI effects were more intense. Hence, HWs exacerbated the UHI effect more during the nighttime and in urbanized areas. In contrast, HWs exacerbated the UHI effect significantly over well-vegetated areas and enhanced the existing cooling island effect.

In contrast, HWs always made the AT higher for the selected sections. During NHWs, the AT of the four sections was 26.95 °C, 28.14 °C, 28.46 °C and 27.35 °C, whereas it reached 27.84 °C, 29.26 °C, 29.68 °C and 28.53 °C, respectively, during HWs (Fig. 4a–d). Larger increases in AT were caused by HWs around 14:00, with greater heat stress. Less urbanized areas had a similar amplification with more urbanized areas at that time. The AT of the four sections increased by 2.12 °C, 1.94 °C, 2.06 °C and 2.25 °C, respectively, at 14:00. However, in the less urbanized area (P2), the increases in AT from midnight to early morning during HWs were much smaller than in the more urbanized areas (P14 and P19). This is consistent with the results of higher temperature and humidity stability in areas with greater vegetation coverage [48], indicating that LULC types also governed interactions between HWs and AT.

3.4. Impact of natural underlying coverage on the interactions between HWs and UHI effect

There were significant negative linear relationships between UHI/AT and natural underlying surface coverage during both HWs and NHWs (Fig. 5a, c, e). As the natural underlying surface coverage increased from 12.43% to 80.12% (coverage of P7; P9 was not included because it was selected as the background section when calculating UHII), the daily, daytime, and nighttime UHII decreased from 1.90 °C, 1.45 °C, and 2.59 °C to −0.30 °C, −0.15 °C, and −0.53 °C in HWs, respectively. The natural underlying surface also significantly decreased AT in HWs and NHWs (Fig. 5b, d, f). With the increase in the underlying surface coverage from 12.43% to 83.13% (P9), the daily, daytime, and nighttime AT decreased from 29.73 °C, 30.55 °C, and 28.48 °C–28.07 °C,

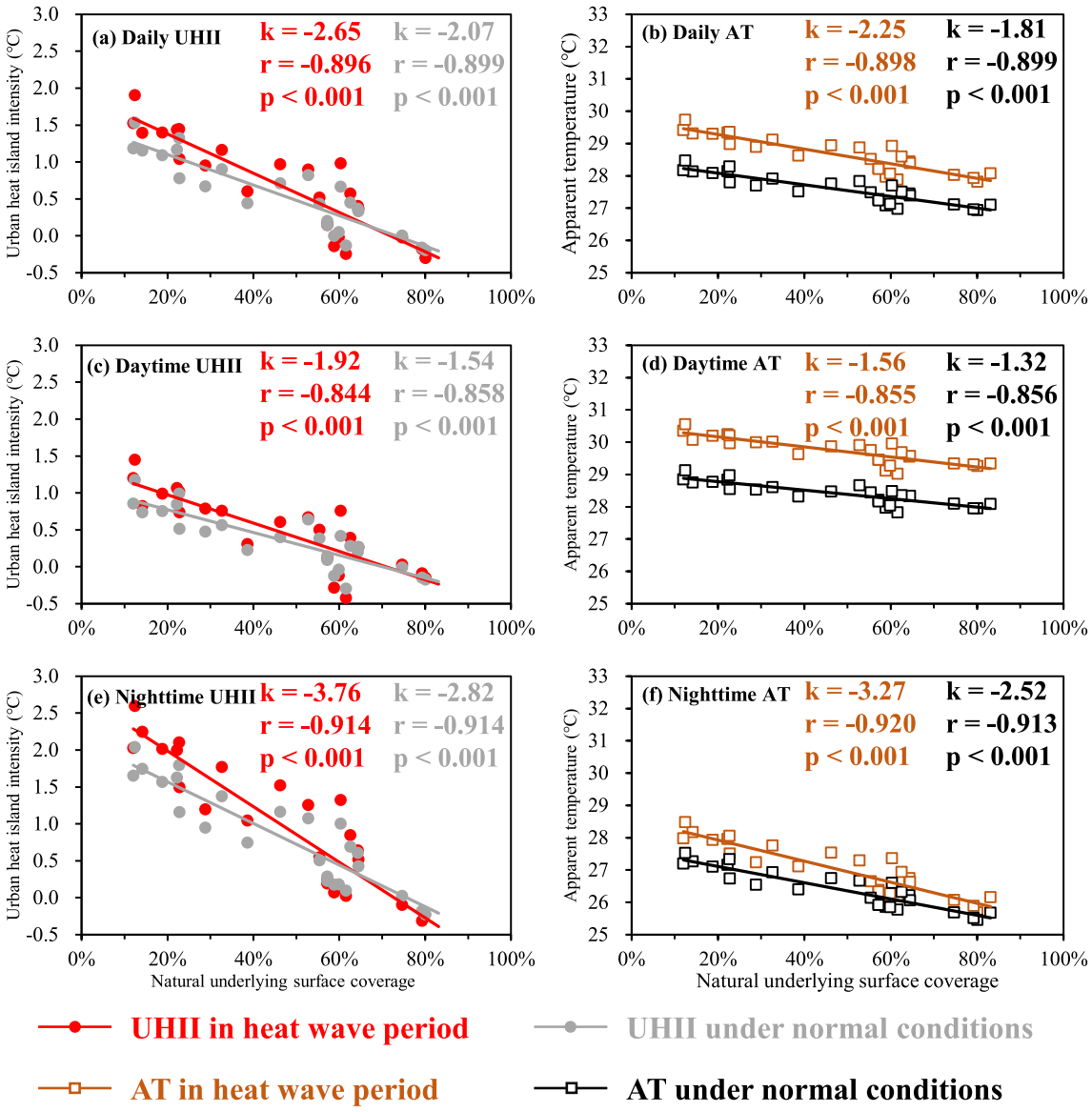

Fig. 5. Impacts of natural underlying surface coverage on urban heat island intensity (UHII) and apparent temperature (AT) during heat wave (HWs) and non-heat waves (NHWs). Impacts on (a, b) daily UHII and AT; (c, d) daytime UHII and AT; (e, f) nighttime UHII and AT, respectively. k is the slope of the regression line, r is the Pearson's correlation coefficient, and p is the correlation significance (95% confidence).

29.34 °C, and 26.16 °C, respectively, during HWs. Therefore, a 10% increase in the vegetated area ratio reduced the nighttime UHII and AT by 0.38 °C and 0.33 °C in HWs and 0.28 °C and 0.25 °C in NHWs, respectively. In addition, the slope was negative throughout the day, regardless of the differences in the determination coefficients. The differences in slopes between HWs and NHWs were significant for daily and nighttime UHII ($p < 0.05$) and nighttime AT ($p < 0.05$). Therefore, HWs significantly enhanced the cooling effects of the natural underlying surface on daily and nighttime UHII, and nighttime AT.

To further investigate the influence of the natural underlying coverage on the interactions between HWs and UHI effects, the relationship between the warming potential (defined as an increase in UHII or AT from NHWs to HWs) and the coverage of the natural underlying surface was analyzed (Fig. 6). The results showed that the natural underlying surface coverage had a significant negative linear influence on the warming potential of UHII and AT. With an increase in the natural underlying surface coverage from 12.43% to 80.12%, the daily, daytime, and nighttime warming potential of UHII decreased from 0.37 °C, 0.27 °C, and 0.56 °C to −0.10 °C, 0.03 °C, and −0.30 °C, respectively. Meanwhile, the daily, daytime, and nighttime warming potential of AT decreased from 1.27 °C, 1.43 °C, and 0.95 °C–0.97 °C, 1.25 °C, and 0.48 °C, respectively. Similar to UHII and AT, the largest mitigation effect of the natural underlying surface coverage on the warming potential of UHII and AT occurred during the nighttime.

4. Discussion

The present study discovered that the cooling effects of the natural underlying surface were always significant, especially at nighttime (Figs. 5 and 6). The cooling effects of the natural underlying surface during the daytime were explained by more latent heat consumption via evapotranspiration [53,54]. However, the incoming energy in more urbanized areas also decreased and warmed the air less, as it could be absorbed and stored by artificial materials [3]. Approximately 20%–30% of short-wave radiation can be stored [55,56]; thus, the cooling effects of the natural underlying surface during the daytime were partly counteracted. However, the stored energy in more urbanized areas was released as long-wave radiation after sunset, which slowed down the

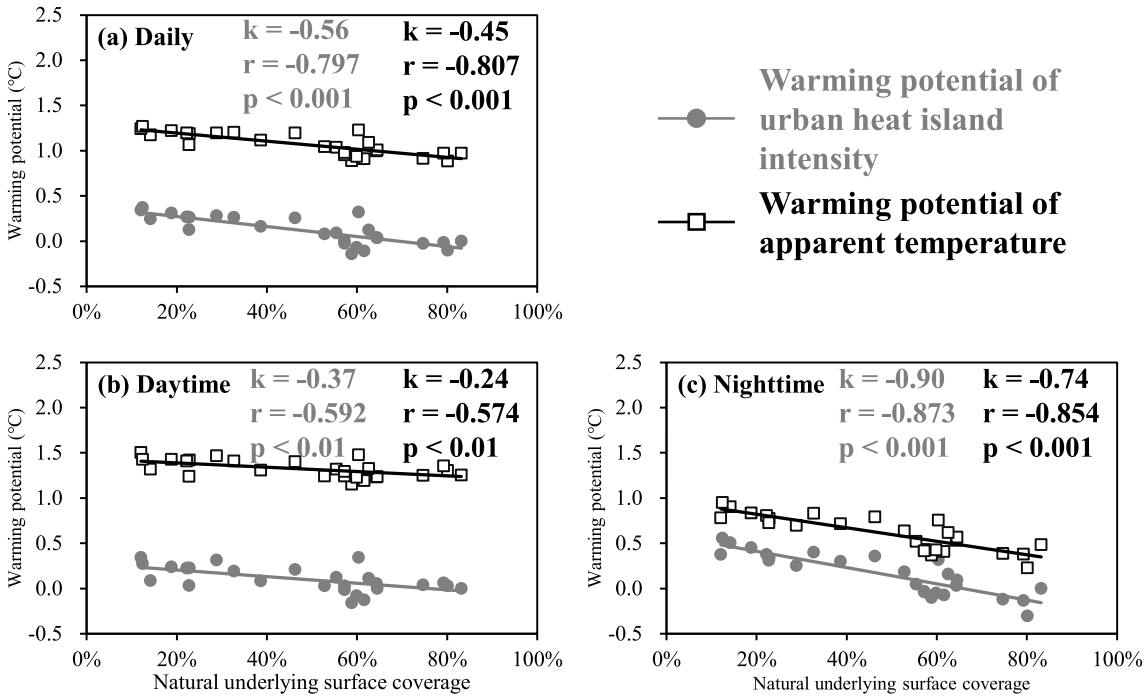

Fig. 6. Cooling effects of the natural underlying surface coverage on urban heat island intensity (UHII) and apparent temperature (AT) (a) daily; (b) in the daytime, and (c) in the nighttime.

cooling process of the air. Lower energy was released at night in less urbanized areas and the air cooled down faster. Therefore, the temperature difference between more and less urbanized areas increased, and the cooling effects of the natural underlying surface became more evident. These results are consistent with those of previous studies [57,58].

The present study found that the UHI effect in the study area became more intense during HWs, and the enhancement was more evident during the nighttime than the daytime, consistent with previous studies conducted in different cities [19–22]. UHII enhancement during the daytime is usually explained by an increased urban-rural contrast in surface evapotranspiration. However, such enhancement at night is associated with greater anthropogenic heat and heat release due to larger heat storage during the daytime [40,59,60]. Radiation, wind speeds, surface moisture, and cloud cover have been identified as factors that affect the interactions between UHI effects and HWs by affecting surface energy exchange [40,59,61,62]. Reduced wind speed was found to be an important reason for UHII exacerbation in HWs, as it could reduce advective cooling by low-temperature air from the surrounding rural areas [40,63]. However, wind speed of our transect during NHWs and NWs were almost the same (1.22 m s^{-1}) based on the adjacent meteorological station data, thus had little impacts on the interactions between UHII and HWs in our study. Our study area could neither be significantly cooled by sea breeze due to enhanced secondary circulations in heat waves [40]. High and dense buildings cut off the sea breeze to our transect. Besides, the sea is to the southeast of our study area while the prevailing wind in summer is from the northeast according to Meteorology Bureau of Shenzhen Municipality [64].

However, in contrast to previous studies conducted at a city scale that documented that HWs would increase or decrease UHII one-sidedly [21,27,59], our high spatial resolution data revealed that the UHI effect had different responses to HWs across different LULC types within a city. The UHII in more urbanized areas was largely higher in HWs than in less urbanized areas. For those areas that already showed cool island effects during NHWs, their cool island intensity was even greater during HWs. Therefore, different measures should be taken for areas with different LULC types within a city to prevent UHI effect from becoming more

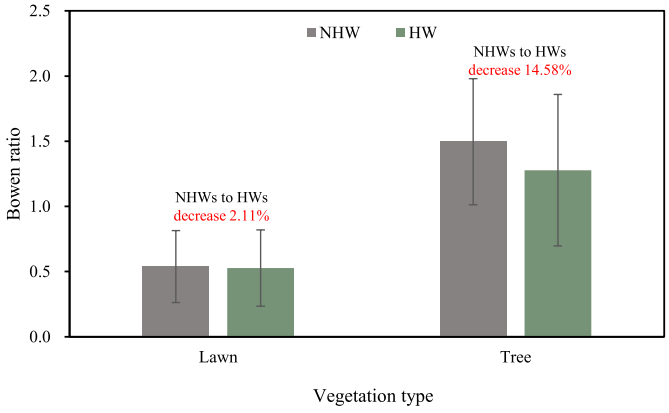

Fig. 7. Bowen ratio (β) of an urban lawn (*Zoysia matrella*) and transpiration rate of an urban tree (*Ficus concinna*) at the university campus (P2) of the transect in four HWs and corresponding NHWs over 2014–2015.

intense during HWs.

Previous studies have shown that the driving force of the interactions between UHI effects and HWs is attributed to the surface energy exchange difference between HWs and NHWs [26–28,36,37], which can explain the different interactions in areas with different LULC types and natural underlying surface coverage. First, more incoming radiation during HWs results in larger radiative energy input, and it becomes warmer in more urbanized areas with some of the increased energy input being transferred into sensible heat. Therefore, HWs lead to a greater increase in UHII in more urbanized areas. Second, as the water supply is usually sufficient during summer in Shenzhen because of ample precipitation [45], there is a high evapotranspiration rate in less urbanized areas during HWs with more energy supply. Thus, consuming more input energy can result in a stronger cool island effect. For example, the urban lawn and urban tree at the university campus site showed lower Bowen ratio during HWs than NHWs, though not significant (Fig. 7). It indicates a greater proportion of net radiation was

consumed by latent heat instead of sensible heat in HWs. Besides, with more input radiation consumed by evapotranspiration in HWs, less heat is stored in less urbanized areas during the daytime, leading to a similar UHII as that during NHWs at nighttime (Fig. 4a). With lower evapotranspiration, pavements or building facets in more urbanized areas store a large part of the input radiation during the daytime and release them at night, leading to a more intense UHI effect (Fig. 4b and c).

Both AT in urbanized areas and less urbanized areas increased in heat waves, because Rothfusz regression (formula 2) was more dependent on air temperature rather than relative humidity in our study area. However, Fig. S1a indicates that the negative impacts of relative humidity on AT are higher just when air temperature and relative humidity are relatively high. The air temperature was between about 28 °C and 32 °C and the relative humidity was between 65% and 80% in our study area (Fig. 2a and b), in which the AT was more decided by the positive impacts of air temperature (Fig. S1b). Thus, AT in more urbanized areas increased significantly in HWs as the air temperature increased a lot. The increase of air temperature and decrease of relative humidity in less urbanized areas were both small in HWs, as vegetation could slow down the warming process and replenish moisture through evapotranspiration. Therefore, the small increase of air temperature also resulted in higher AT.

Our research also indicated that there was a negative linear relationship between the natural underlying surface coverage and UHI/AT during HWs and NHWs. The cooling effects of the underlying surface coverage, particularly vegetation coverage, are consistent with most previous studies in which HWs and NHWs were not distinguished [30,31,54,65,66]. The present study demonstrated that the absolute value of the slope was larger during HWs, indicating that the cooling effect of the natural underlying surface was enhanced by HWs. This could also be explained by the different responses of energy exchange to HWs. More natural underlying surfaces mean more latent heat consumption and less heat storage release. Consequently, the warming potential of UHII/AT during HWs decreased with the coverage of the natural underlying surface. These findings imply that the natural underlying surface plays an important role in stabilizing the thermal environment, thus reducing the adverse influence of HWs. Therefore, as one of the most economical and effective natural underlying surfaces, more vegetation is a feasible method to mitigate the amplification of UHI effects in HWs, and create a better thermal environment for urban areas.

5. Conclusions

The interactions between UHI effects and HWs have drawn much attention recently due to increased urbanization and global warming. Our research, based on high spatial-temporal resolution data from a mobile transect observation, showed that the UHI effect was exacerbated during HWs in the subtropical megacity of Shenzhen. The UHII of the transect increased from 0.56 °C during NHWs to 0.68 °C during HWs. However, LULC types significantly affected this interaction, with the UHII in more urbanized areas increasing more during HWs and less urbanized areas receiving better cooling effects. These amplifications were more evident at nighttime, highlighting that mitigation measures should focus on the nighttime UHI effect of more urbanized areas. Increasing the natural underlying surface coverage could mitigate the intensity and warming potential of UHI effects, especially at nighttime. With the increase in the natural underlying surface coverage from 12.43% to 80.12%, the daily, daytime, and nighttime UHII decreased from 1.90 °C, 1.45 °C, and 2.59 °C to −0.30 °C, −0.15 °C, and −0.53 °C, respectively, during HWs. These cooling effects may be attributed to the increased latent heat consumption during HWs by vegetation. With an increasing frequency of HWs, exacerbation of the thermal environment is inevitable. However, measures can be taken to mitigate further increases in the UHI effect. These measures could differ in different areas of a city. Nevertheless, the most important measure is to discourage global warming and have fewer HWs, which requires worldwide effort.

Declaration of competing interest

The authors declare that they have no known competing financial interests or personal relationships that could have appeared to influence the work reported in this paper.

Acknowledgement

We acknowledge, with gratitude, the financial support from National Natural Science Foundation of China (42001022), and Science and Technology Planning Project of Shenzhen Municipality (JCYJ20180504165440088, GXWD20201231165807007-20200827105738001). The authors would like to express their great thanks to Shuishan Wang, Hongyong Li, Xiangze Li, Yekui Yu, Qiuping Guo, Xianglin Hao, and Jiao Xiang for their contributions during the field experiment. Thanks are also extended to Dr. Muhammad Hayat and Elsevier Language Editing Service for their efforts to improve the grammar of this paper.

Appendix A. Supplementary data

Supplementary data to this article can be found online at https://doi.org/10.1016/j.buildenv.2021.108138.

References

[1] N.B. Grimm, S.H. Faeth, N.E. Golubiewski, C.L. Redman, J. Wu, X. Bai, J.M. Briggs, Global change and the ecology of cities, Science 319 (5864) (2008) 756–760, https://doi.org/10.1126/science.1150195.
[2] United Nations Population Division, World Urbanization Prospects 2018, 2019. https://population.un.org/wup/Download. (Accessed 2 April 2021).
[3] A.M. Rizwan, L.Y. Dennis, C. Liu, A review on the generation, determination and mitigation of urban heat island, J. Environ. Sci. 20 (2008) 120–128, https://doi.org/10.1016/S1001-0742(08)60019-4, 001.
[4] J. Wang, W. Zhou, P. Sta, W. Yu, W. Li, A multiscale analysis of urbanization effects on ecosystem services supply in an urban megaregion, Sci. Total Environ. 662 (2019) 824–833, https://doi.org/10.1016/j.scitotenv.2019.01.260.
[5] K. Gobakis, D. Kolokotsa, A. Synnefa, M. Saliari, M. Santamouris, Development of a model for urban heat island prediction using neural network techniques, Sust. Cities Soc. 1 (2) (2011) 104–115, https://doi.org/10.1016/j.scs.2011.05.001.
[6] J. Tan, Y. Zheng, T. Xu, C. Guo, L. Li, G. Song, X. Zhen, Y. Dong, A.J. Kalkstein, F. Li, The urban heat island and its impact on heat waves and human health in Shanghai, Int. J. Biometeorol. 54 (1) (2010) 75–84, https://doi.org/10.1007/s00484-009-0256-x.
[7] Z. Gou, S. Lau, P. Lin, Understanding domestic air-conditioning use behaviours: disciplined body and frugal life, Habitat Int. 60 (2017) 50–57, https://doi.org/10.1016/j.habitatint.2016.12.009.
[8] A.H. Rosenfeld, H. Akbari, J.J. Romm, Cool communities: strategies for heat island mitigation and smog reduction, Energy Build. 28 (1) (1998) 51–62, https://doi.org/10.1016/S0378-7788(97)00063-7.
[9] C. De Munck, G. Pigeon, V. Masson, F. Meunier, P. Bousquet, B. Tréméac, M. Merchat, P. Poeuf, C. Marchadier, How much can air conditioning increase air temperatures for a city like Paris, France? Int. J. Climatol. 33 (2013) 210–227, https://doi.org/10.1002/joc.3415.
[10] E. Stathopoulou, G. Mihalakakou, M. Santamouris, H.S. Bagiorgas, On the impact of temperature on tropospheric ozone concentration levels in urban environments, J. Earth Syst. Sci. 117 (3) (2008) 227–236, https://doi.org/10.1007/s12040-008-0027-9.
[11] E. Xoplaki, J.F. Gonzalez-Rouco, J. Luterbacher, H. Wanner, Mediterranean summer air temperature variability and its connection to the large-scale atmospheric circulation and SSTs, Clim. Dynam. 20 (2003) 723–739, https://doi.org/10.1007/s00382-003-0304-x.
[12] E. Black, M. Blackburn, G. Harrison, B. Hoskins, J. Methven, Factors contributing to the summer 2003 European heatwave, Weather 59 (8) (2004) 217–223, https://doi.org/10.1256/wea.74.04.
[13] D. Coumou, S. Rahmstorf, A decade of weather extremes, Nat. Clim. Change 2 (7) (2012) 491–496, https://doi.org/10.1038/NCLIMATE1452.
[14] C. Schaer, P.L. Vidale, D. Luethi, C. Frei, C. Haeberli, M.A. Liniger, C. Appenzeller, The role of increasing temperature variability in European summer heatwaves, Nature 427 (6972) (2004) 332–336, https://doi.org/10.1038/nature02300.
[15] N.C. Lau, M.J. Nath, Model simulation and projection of European heat waves in present-day and future climates, J. Clim. 27 (10) (2014) 3713–3730, https://doi.org/10.1175/JCLI-D-13-00284.1.
[16] R.M. Horton, C. Lesk, J.S. Mankin, A review of recent advances in research on extreme heat events, Curr. Clim. Chang. Rep. 2 (4) (2016) 242–259, https://doi.org/10.1007/s40641-016-0042-x.
[17] G.A. Meehl, C. Tebaldi, More intense, more frequent, and longer lasting heat waves in the 21st century, Science 305 (5686) (2004) 994–997, https://doi.org/10.1126/science.1098704.

[18] X. Yang, L.R. Leung, N. Zhao, C. Zhao, Q. Yun, K. Hu, X. Liu, B. Chen, Contribution of urbanization to the increase of extreme heat events in an urban agglomeration in East China, Geophys. Res. Lett. 44 (13) (2017) 6940–6950, https://doi.org/10.1002/2017GL074084.
[19] P. Ramamurthy, E. Bou-Zeid, Heatwaves and urban heat islands: a comparative analysis of multiple cities, J. Geophys. Res. Atmos. 122 (1) (2017) 168–178, https://doi.org/10.1002/2016JD025357.
[20] P. Ramamurthy, D. Li, E. Bou-Zeid, High-resolution simulation of heatwave events in New York City, Theor. Appl. Climatol. 128 (1–2) (2015) 1–14, https://doi.org/10.1007/s00704-015-1703-8.
[21] S. Jiang, X. Lee, J. Wang, K. Wang, Amplified urban heat islands during heat wave periods, J. Geophys. Res. Atmos. 124 (14) (2019) 7797–7812, https://doi.org/10.1029/2018JD030230.
[22] X. He, J. Wang, J. Feng, Z. Yan, J. Xia, Observational and modeling study of interactions between urban heat island and heatwave in Beijing, J. Clean. Prod. 247 (2020) 119169, https://doi.org/10.1016/j.jclepro.2019.119169.
[23] S.H. Rizvi, K. Alam, M.J. Iqbal, Spatio -temporal variations in urban heat island and its interaction with heat wave, J. Atmos. Sol. Terr. Phys. 185 (2019) 50–57, https://doi.org/10.1016/j.jastp.2019.02.001.
[24] J. Unger, N. Skarbit, A. Kovács, T. Gál, Comparison of regional and urban outdoor thermal stress conditions in heatwave and normal summer periods: a case study, Urban Clim. 32 (2020) 100619, https://doi.org/10.1016/j.uclim.2020.100619.
[25] L.W. Chew, X. Liu, X. Li, L.K. Norford, Interaction between heat wave and urban heat island: a case study in a tropical coastal city, Singapore, Atmos. Res. 247 (2021) 105134, https://doi.org/10.1016/j.atmosres.2020.105134.
[26] A.A. Scott, D.W. Waugh, B.F. Zaitchik, Reduced urban heat island intensity under warmer conditions, Environ. Res. Lett. 13 (2018), 064003, https://doi.org/10.1088/1748-9326/aabd6c.
[27] L. Zhao, M. Oppenheimer, Q. Zhu, J.W. Baldwin, K.L. Ebi, E. Bou-Zeid, K. Guan, X. Liu, Interactions between urban heat islands and heat waves, Environ. Res. Lett. 13 (3) (2018), 034003, https://doi.org/10.1088/1748-9326/aa9f73.
[28] W. Liao, X. Liu, D. Li, M. Luo, D. Wang, S. Wang, J. Baldwin, L. Lin, X. Li, K. Feng, K. Hubacek, X. Yang, Stronger contributions of urbanization to heat wave trends in wet climates, Geophys. Res. Lett. 45 (20) (2018) 11310–11317, https://doi.org/10.1029/2018GL079679.
[29] N. Harmay, D. Kim, M. Choi, Urban heat island associated with land use/land cover and climate variations in Melbourne, Australia, Sust. Cities Soc. 69 (2021) 102861, https://doi.org/10.1016/j.scs.2021.102861.
[30] G. Guo, Z. Wu, R. Xiao, Y. Chen, X. Liu, X. Zhang, Impacts of urban biophysical composition on land surface temperature in urban heat island clusters, Landsc. Urban Plann. 135 (2015) 1–10, https://doi.org/10.1016/j.landurbplan.2014.11.007.
[31] C.W. Mackey, X. Lee, R.B. Smith, Remotely sensing the cooling effects of city scale efforts to reduce urban heat island, Build. Environ. 49 (2012) 348–358, https://doi.org/10.1016/j.buildenv.2011.08.004.
[32] M. Mohan, Y. Kikegawa, B.R. Gurjar, S. Bhati, N.R. Kolli, Assessment of urban heat island effect for different land use–land cover from micrometeorological measurements and remote sensing data for megacity Delhi, Theor. Appl. Climatol. 112 (3–4) (2003) 647–658, https://doi.org/10.1007/s00704-012-0758-z.
[33] J. Unger, Z. Sümeghy, J. Zoboki, Temperature cross-section features in an urban area, Atmos. Res. 58 (2) (2001) 117–127, https://doi.org/10.1016/S0169-8095(01)00087-4.
[34] G.L. Feyisa, K. Dons, H. Meilby, Efficiency of parks in mitigating urban heat island effect: an example from Addis Ababa, Landsc. Urban Plann. 123 (2) (2014) 87–95, https://doi.org/10.1016/j.landurbplan.2013.12.008.
[35] S. Hamada, T. Ohta, Seasonal variations in the cooling effect of urban green areas on surrounding urban areas, Urban For. Urban Gree. 9 (1) (2010) 15–24, https://doi.org/10.1016/j.ufug.2009.10.002.
[36] K. Abutaleb, A. Ngie, A. Darwish, M. Ahmed, F. Ahmed, Assessment of urban heat island using remotely sensed imagery over Greater Cairo, Egypt, Adv. Rem. Sens. 4 (4) (2015) 35–47, https://doi.org/10.4236/ars.2015.41004.
[37] B.C. Mitchell, J. Chakraborty, Urban heat and climate justice: a landscape of thermal inequity in Pinellas County, Florida, Geogr. Rev. 104 (4) (2014) 459–480, https://doi.org/10.1111/j.1931-0846.2014.12039.x.
[38] M. Mohan, Y. Kikegawa, B.R. Gurjar, S. Bhati, N.R. Kolli, Assessment of urban heat island effect for different land use–land cover from micrometeorological measurements and remote sensing data for megacity Delhi, Theor. Appl. Climatol. 112 (3–4) (2013) 647–658, https://doi.org/10.1007/s00704-012-0758-z.
[39] A.S. Yang, Y.H. Juan, C.Y. Wen, C.J. Chang, Numerical simulation of cooling effect of vegetation enhancement in a subtropical urban park, Appl. Energy 192 (2017) 178–200, https://doi.org/10.1016/j.apenergy.2017.01.079.
[40] D. Li, E. Bou-Zeid, Synergistic interactions between urban heat islands and heat waves: the impact in cities is larger than the sum of its parts*, J. Appl. Meteorol. Climatol. 52 (9) (2013) 2051–2064, https://doi.org/10.1175/JAMC-D-13-02.1.
[41] X. Ao, L. Wang, X. Zhi, W. Gu, D. Li, Observed Synergies between urban heat islands and heat waves and their controlling factors in Shanghai, China, J. Appl. Meteorol. Clim. 58 (9) (2019) 1955–1972, https://doi.org/10.1175/JAMC-D-19-0073.1.
[42] E.M. Fischer, C. Schär, Consistent geographical patterns of changes in high-impact European heatwaves, Nat. Geosci. 3 (2010) 398–403, https://doi.org/10.1038/ngeo866.
[43] G.R. Steadman, The assessment of sultriness. part I: a temperature-humidity index based on human physiology and clothing science, J. Appl. Meteorol. 18 (7) (1979) 861–873, https://doi.org/10.1175/1520-0450(1979)018<0861:TAOSPI>2.0.CO;2.
[44] Q. Guo, Impacts of Vegetation Coverage on Urban Thermal Environment and Thermal Comfort-Case Study of Shenzhen, School of Environment and Energy, Peking University, 2015 (Master Degree dissertation).
[45] M.A. Hart, D.J. Sailor, Quantifying the influence of land-use and surface characteristics on spatial variability in the urban heat island, Theor. Appl. Climatol. 95 (3) (2009) 397–406, https://doi.org/10.1007/s00704-008-0017-5.
[46] M. Yokohari, R.D. Brown, Y. Kato, S. Yamamoto, The cooling effect of paddy fields on summertime air temperature in residential Tokyo, Japan, Landsc. Urban Plann. 53 (1) (2001) 17–27, https://doi.org/10.1016/S0169-2046(00)00123-7.
[47] G.Y. Qiu, Z. Zou, X. Li, H. Li, Q. Guo, C. Yan, S. Tan, Experimental studies on the effects of green space and evapotranspiration on urban heat island in a subtropical megacity in China, Habitat Int. 68 (2017) 30–42, https://doi.org/10.1016/j.habitatint.2017.07.009.
[48] C. Yan, Q. Guo, H. Li, L. Li, G.Y. Qiu, Quantifying the cooling effect of urban vegetation by mobile traverse method: a local-scale urban heat island study in a subtropical megacity, Build. Environ. 169 (2020) 106541, https://doi.org/10.1016/j.buildenv.2019.106541.
[49] G. Qiu, S. Tan, W. Yue, X. Yu, C. Yan, Characteristics of evapotranspiration of urban lawns in a sub-tropical megacity and its measurement by the 'Three Temperature Model + Infrared Remote Sensing' method, Rem. Sens. 9 (2017) 502, https://doi.org/10.3390/rs9050502.
[50] G.Y. Qiu, X. Yu, H. Wen, C. Yan, An advanced approach for measuring the transpiration rate of individual urban trees by the 3D three-temperature model and thermal infrared remote sensing, J. Hydrol. 587 (2020) 125034, https://doi.org/10.1016/j.jhydrol.2020.125034.
[51] L.P. Rothfusz, The heat index equation (or, more than you ever wanted to know about heat index), in: National Weather Service Technical Attachment, Scientific Services Division NWS Southern Region Headquarters, TX, SR: Fort Worth, 1990. SR/SSD 90-23.
[52] F. Kong, H. Yin, P. James, L.R. Hutyra, H.S. He, Effects of spatial pattern of greenspace on urban cooling in a large metropolitan area of eastern China, Landsc. Urban Plann. 128 (3) (2014) 35–47, https://doi.org/10.1016/j.landurbplan.2014.04.018.
[53] A. Sharma, P. Conry, H. Fernando, A.F. Hamlet, J.J. Hellmann, F. Chen, Green and cool roofs to mitigate urban heat island effects in the Chicago metropolitan area: evaluation with a regional climate model, Environ. Res. Lett. 11 (6) (2016), 064004, https://doi.org/10.1088/1748-9326/11/6/064004.
[54] C.D. Ziter, E.J. Pedersen, C.J. Kucharik, M.G. Turner, Scale-dependent interactions between tree canopy cover and impervious surfaces reduce daytime urban heat during summer, Proc. Natl. Acad. Sci. U. S. A 116 (15) (2019) 7575–7580, https://doi.org/10.1073/pnas.1817561116.
[55] T.R. Oke, H.A. Cleugh, Urban heat storage derived as energy balance residuals, Boundary-Layer Meteorol. 39 (3) (1987) 233–245, https://doi.org/10.1007/bf00116120.
[56] W.D. Solecki, C. Rosenzweig, L. Parshall, G. Pope, M. Clark, J. Cox, M. Wiencke, Mitigation of the heat island effect in urban New Jersey, Glob. Environ. Chang. B Environ. Hazards 6 (1) (2005) 39–49, https://doi.org/10.1016/j.hazards.2004.12.002.
[57] N.H. Wong, C. Yu, Study of green areas and urban heat island in a tropical city, Habitat Int. 29 (3) (2005) 547–558, https://doi.org/10.1016/j.habitatint.2004.04.008.
[58] T. Yokobori, S. Ohta, Effect of land cover on air temperatures involved in the development of an intra-urban heat island, Clim. Res. 39 (1) (2009) 61–73, https://doi.org/10.3354/cr00800.
[59] D. Li, T. Sun, M. Liu, L. Yang, L. Wang, Z. Gao, Contrasting responses of urban and rural surface energy budgets to heat waves explain synergies between urban heat islands and heat waves, Environ. Res. Lett. 10 (5) (2015), 054009, https://doi.org/10.1088/1748-9326/10/5/054009.
[60] T. Sun, S. Kotthaus, D. Li, H.C. Ward, Z. Gao, G. Ni, S. Grimmond, Attribution and mitigation of heat wave-induced urban heat storage change, Environ. Res. Lett. 12 (11) (2017) 114007, https://doi.org/10.1088/1748-9326/aa922a.
[61] A.J. Arnfield, Two decades of urban climate research: a review of turbulence, exchanges of energy and water, and the urban heat island, Int. J. Climatol. 23 (1) (2003) 1–26, https://doi.org/10.1002/joc.859.
[62] D. Li, T. Sun, M. Liu, L. Wang, Z. Gao, Changes in wind speed under heat waves enhance urban heat islands in the Beijing Metropolitan Area, J. Appl. Meteorol. Climatol. 55 (11) (2016) 2369–2375, https://doi.org/10.1175/JAMC-D-16-0102.1.
[63] T.R. Oke, The energetic basis of the urban heat island, Q. J. R. Meteorol. Soc. 108 (455) (1982) 1–24, https://doi.org/10.1002/qj.49710845502.
[64] Meteorology Bureau of Shenzhen Municipality, Overview of Shenzhen's Climate and Characteristics of Four Seasons, 2021. http://weather.sz.gov.cn/qixiangfuwu/qihoufuwu/qihouguanceyupinggu/qihougaikuang/index.html. (Accessed 7 July 2021).
[65] A. Mathew, S. Khandelwal, N. Kaul, Spatial and temporal variations of urban heat island effect and the effect of percentage impervious surface area and elevation on land surface temperature: study of Chandigarh city, India, Sust. Cities Soc. 26 (2016) 264–277, https://doi.org/10.1016/j.scs.2016.06.018.
[66] W. Zhou, J. Wang, M.L. Cadenasso, Effects of the spatial configuration of trees on urban heat mitigation: a comparative study, Remote Sens. Environ. 195 (2017) 1–12, https://doi.org/10.1016/j.rse.2017.03.043.